Observations of Vortex Rossby Waves Associated with a Mesoscale Cyclone*

CÉDRIC P. CHAVANNE,+ PIERRE FLAMENT, AND DOUGLAS S. LUTHER

School of Ocean and Earth Science and Technology, University of Hawaii at Manoa, Honolulu, Hawaii

KLAUS-WERNER GURGEL

Institute of Oceanography, University of Hamburg, Hamburg, Germany

(Manuscript received 27 April 2010, in final form 25 June 2010)

ABSTRACT

Short-wavelength ($L \sim 100$ km) Rossby waves with an eastward zonal phase velocity were observed by high-frequency radio Doppler current meters and moored ADCPs west of Oahu, Hawaii, during spring 2003. They had Rossby numbers $\mathrm{Ro} = |\zeta/f| = O(1)$, periods of 12–15 days, and phase speeds of 8–9 cm s^{-1}, and they were surface trapped with vertical *e*-folding scales of 30–170 m. They transferred horizontal kinetic energy to the background flow of a mesoscale cyclone lying 160–190 km west of Oahu, revealed by altimetry. The waves approximately satisfied the dispersion relation of vortex Rossby waves propagating through the radial gradient of potential vorticity associated with the cyclone. Vertical shear of the background currents may also affect wave propagation. Theoretical studies have shown that vortex Rossby waves provide a mechanism by which perturbed vortices axisymmetrize and strengthen and may be important to the dynamics of oceanic vortices.

1. Introduction

Waves propagating through the radial gradient of the potential vorticity field associated with vortices are called vortex Rossby waves (VRW), and they were first proposed to describe hurricane spiral bands (MacDonald 1968). VRW theory was subsequently developed to understand the response of atmospheric cyclones to asymmetric perturbations. VRWs provide a mechanism by which perturbed vortices axisymmetrize and strengthen (Montgomery and Kallenbach 1997; Möller and Montgomery 1999; McWilliams et al. 2003; Graves et al. 2006), and remain vertically aligned when subjected to vertical shear perturbations (Reasor and Montgomery 2001). VRWs may be associated with oceanic vortices as well but require high-resolution observations to be detected.

Oceanic observations of Rossby waves have tended to focus on long wavelengths ($L \gtrsim 200$ km) because of the generally low spatial resolution of measurements such as arrays of in situ instruments (e.g., Chave et al. 1992) or satellite altimetry (e.g., Chelton and Schlax 1996) or simply because of the dynamical nature of the observed phenomenon, such as annual Rossby waves in the tropical North Pacific (White 1977) or meanders of frontal jets (e.g., Hansen 1970; Tracey et al. 2006). Here, we describe high-resolution (2 km) observations by high-frequency radio (HFR) Doppler current meters and moored acoustic Doppler current profilers (ADCP), revealing short-wavelength ($L \sim 100$ km) VRWs that dominated the subinertial near-surface variability west of Oahu, Hawaii, during March and April 2003.

2. Methods

Two 16-MHz HFR Doppler current meters were deployed (Fig. 1) from September 2002 to May 2003, providing 2-km-resolution hourly surface currents (for a description of the processing, see Chavanne et al. 2010b). Also, 300- and 75-kHz ADCPs were moored looking

* University of Hawaii at Manoa School of Ocean and Earth Science and Technology Contribution Number 7919.

+ Current affiliation: School of Environmental Sciences, University of East Anglia, Norwich, United Kingdom.

Corresponding author address: Cédric Chavanne, School of Environmental Sciences, University of East Anglia, Norwich NR4 7TJ, United Kingdom.
E-mail: cedric.chavanne@ensta.org

DOI: 10.1175/2010JPO4495.1

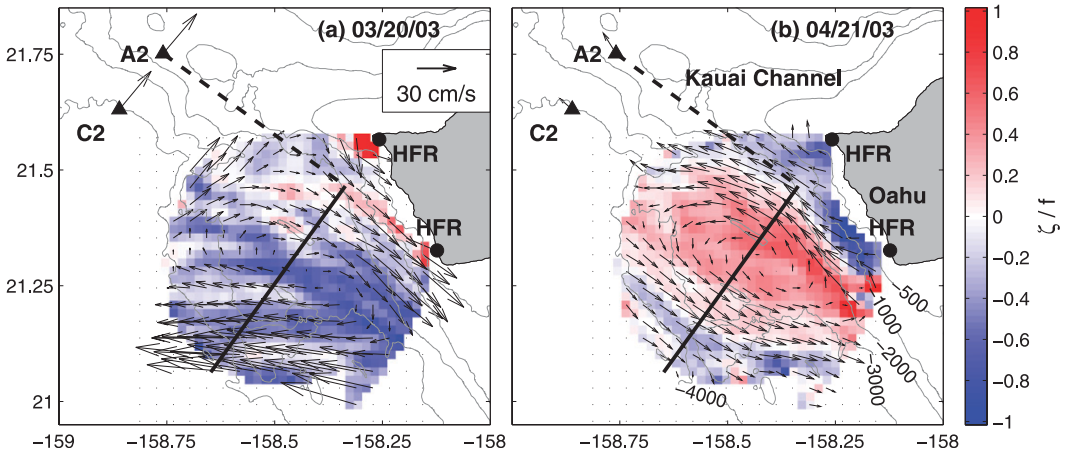

FIG. 1. Snapshots of low-pass filtered surface current anomalies from HFRs (marked by black bullets) and ADCPs moored at A2 and C2 (12-m depth; marked by black triangles), on (a) 20 Mar (mean currents from 14 to 30 Mar were subtracted) and (b) 21 Apr (mean currents from 13 to 25 Apr were subtracted) 2003. Vorticity is normalized by f. Bathymetric contours are labeled in meters. The solid black lines, heading 234°–54° and perpendicular to the nearshore currents, indicate the transect displayed in Fig. 2; the normal at the origin of the transect (dashed black line) intersects A2. Distance along the transect is taken as positive northeastward.

upward in the Kauai Channel, at mooring C2 (21.63°N, 158.86°W) in 4010-m bottom depth and at mooring A2 (21.75N, 158.76W) in 1330-m bottom depth (Fig. 1), from November 2002 to June 2003. The ADCPs covered depth ranges of 12–80 m at each mooring with 4-m vertical resolution and of 200–720 m at C2 and 160–1296 m at A2 with 8-m vertical resolution. The 10-min sample ensembles were averaged hourly.

The ADCPs were outside the domain covered by HFR vector currents but within the domain of radial currents from the southern HFR. Correlations between ADCP currents at 12-m depth, projected onto the directions toward the southern HFR, and the HFR surface radial currents were ~0.9, with rms differences of ~11 cm s^{-1}. The HFR and ADCP currents were low-pass filtered with a 4-day cutoff period to remove tides, near-inertial oscillations, and island-trapped Kelvin waves (for details, see Chavanne et al. 2010a).

The larger-scale context is provided by geostrophic currents inferred from satellite altimetry on a 33-km grid (Ducet et al. 2000), produced by Ssalto/Duacs and distributed by the Archiving, Validation, and Interpretation of Satellite Oceanographic data (AVISO; available online at http://www.aviso.oceanobs.com/).

3. Observations

From March to April 2003, subinertial currents south of the Kauai Channel were dominated by Rossby waves. Two snapshots about 180° out of phase are shown in Fig. 1. On 20 March (Fig. 1a), currents varied from westward to southeastward between the southwest and northeast parts of the domain, resulting in a negative vorticity band $O(f)$ aligned in the northwest–southeast direction. On 21 April (Fig. 1b), the pattern was reversed and extended northwestward to the moorings.

These patterns propagated to the northeast, as seen for the current component normal to the propagation direction (Fig. 2b), ~90° off the mean current direction (Figs. 3a, 4a), suggesting that they were Rossby waves rather than isolated elongated eddies advected by the mean flow. Furthermore, during April 2003, the northwest–southeast near-surface velocity component at A2 (Fig. 2c) and near the coast (Fig. 2b at 0 km) were correlated, corroborating the approximate plane wave structure displayed in Fig. 1b. The current component parallel to the propagation direction (Fig. 2a) should be small for Rossby waves and is probably dominated by other processes here, which do not propagate with the waves. The structure was more complex during March 2003, when the currents in the northwestern part of the domain were northeastward (Fig. 1a). The vertical structures also differed between March and April 2003: they were both surface intensified, but the vertical decay scale was shorter in April than in March (Figs. 2c,d).

To analyze these differences, the wave structures will be quantitatively characterized during the following two time segments (delimited by vertical solid lines in Fig. 2): 14–30 March (period 1) and 13–25 April (period 2). Each segment encompasses a full wave period. Two complementary analyses will be performed: a Radon transform (RT; Challenor et al. 2001) on the vorticity field, and a complex empirical orthogonal function (CEOF) decomposition of the current field (Barnett 1983).

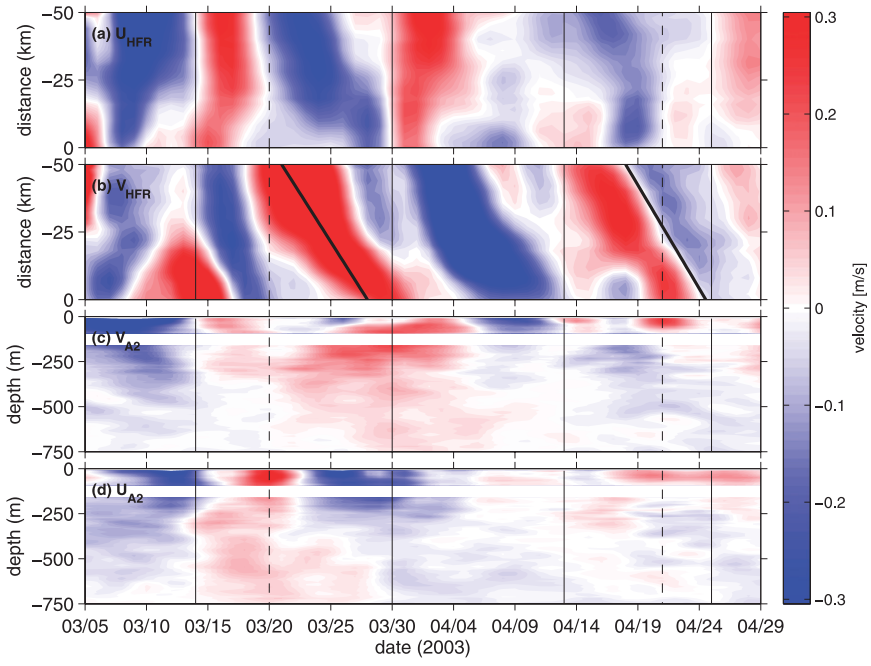

FIG. 2. Time series of (a),(b) surface current anomalies as a function of distance along the transect shown in Fig. 1, and (c),(d) current anomalies at mooring A2 as a function of depth, decomposed in (a),(d) along-transect U and (b),(c) across-transect V components. The mean currents from 5 Mar to 29 Apr were subtracted. The vertical dashed lines indicate the times of the snapshots shown in Fig. 1, and the vertical solid lines indicate the intervals of the periods of the analysis. The slanted bold lines represent the phase propagation inferred from the RTs.

RTs can be used to infer the direction and velocity of propagation of wave-like signals in three dimensions (e.g., longitude, latitude, time). First, a scalar field ζ (relative vorticity) is projected onto an azimuthal direction ϕ, yielding a 2D (distance and time) scalar field $\overline{\zeta}$. Then, $\overline{\zeta}$ is projected onto a direction θ in the 2D plane, yielding a 1D scalar field $\tilde{\zeta}$, the variance of which gives the energy of the signal for the chosen ϕ and θ angles. The values of ϕ and θ for which the energy is at maximum yield the azimuthal direction and velocity of propagation of the waves, respectively. This method yields phase velocities, periods, and wavelengths of 8.0 cm s^{-1}, 14.8 days, and 102 km during period 1 and 8.6 cm s^{-1}, 11.7 days, and 87 km during period 2.

CEOF analysis of HFR and ADCP currents provide a picture of both horizontal and vertical structures of the waves. In contrast to standard EOF analysis, CEOFs are capable of detecting propagating features, by using the Hilbert transform to retain both co-phase and quadrature-phase information on the signals. The waves were captured by the first CEOF, which contained 88% and 87% of the subinertial kinetic energy during periods 1 and 2 (Figs. 3, 4).

During period 1, surface currents in the southwestern part of the domain were zonally polarized (Fig. 3c), and they were oriented 40°–50° counterclockwise from the mean flow direction (Fig. 3a). They were less polarized closer to shore. The amplitude of vorticity fluctuations (Fig. 3c) reached $O(f)$ near the coast. The spatial phase (Fig. 3d) indicates a northeastward propagation, with a gradual turning and increase of local wavenumbers toward the coast, suggesting refraction by topography. The local wavelengths and instantaneous periods ranged from 50 to 250 km and from 12.5 to 19 days (Fig. 3f), bracketing the values estimated from the RT. The wave amplitude was surface intensified (Fig. 3b) and decayed below a surface layer ~40-m thick, with an e-folding scale $H = 170$ m. The mean currents decayed more slowly with depth.

During period 2, surface currents were polarized in the northwestward direction over most of the domain, including the moorings (Fig. 4c), and oriented 20°–35° counterclockwise from the mean flow (Fig. 4a). The spatial phase (Fig. 4d) indicates again a northeastward propagation, but it is less affected by topography than during period 1. The local wavelengths ranged from 25 to 150 km, bracketing the 87 km obtained from the RT. The instantaneous period (Fig. 4f) stabilized around 11.1 days when the amplitude was high, close to the 11.7 days estimated from the RT. The current amplitudes were surface intensified (Fig. 4b) and strongly sheared

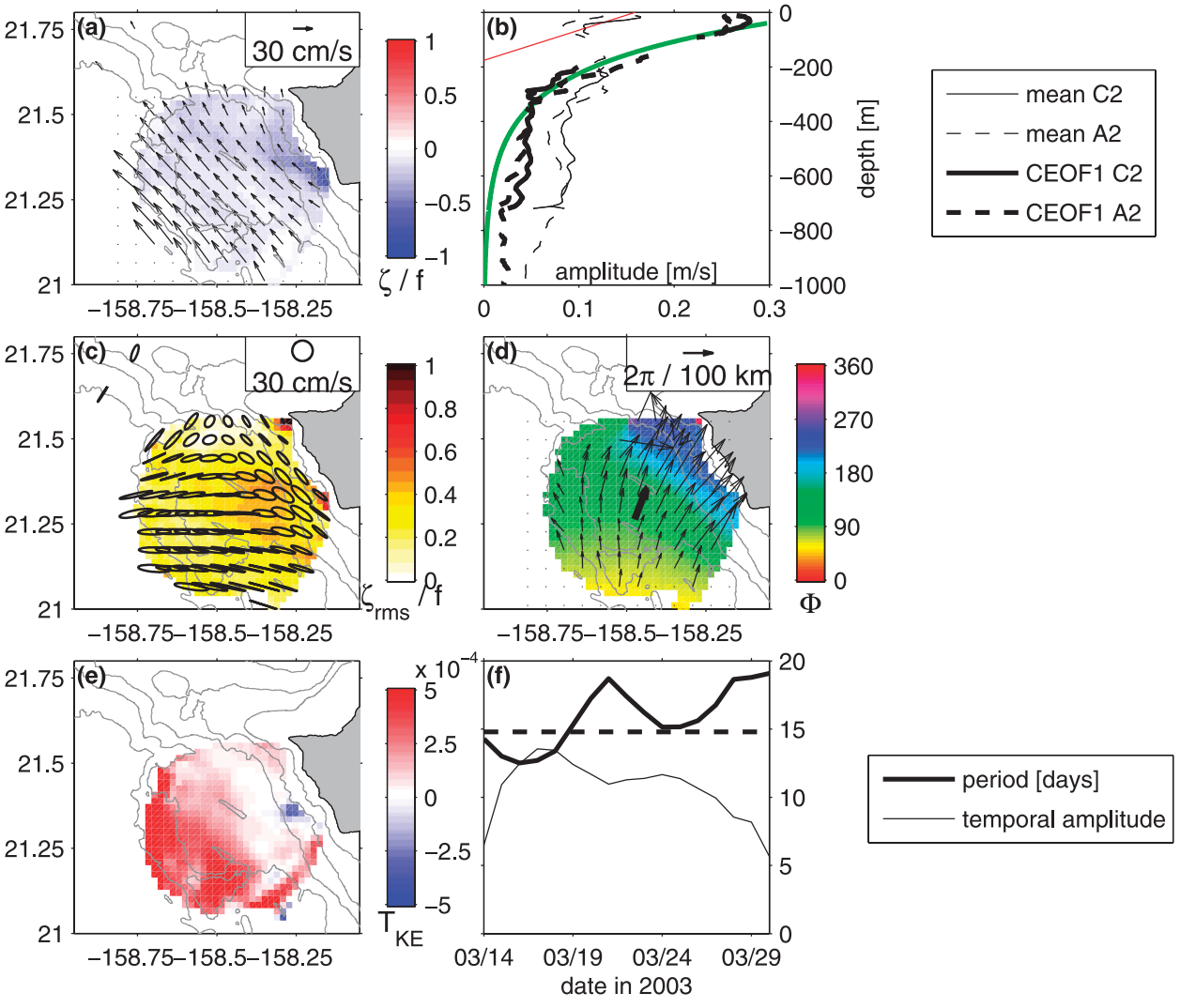

FIG. 3. First CEOF for period 1: (a) mean currents and vorticity (normalized by f), subtracted before computing the CEOFs; (b) vertical profiles of current magnitude at C2 (solid black lines) and A2 (dashed black lines) for the mean (thin lines) and CEOF 1 (bold lines) currents; (c) horizontal structure of currents and standard deviation of vorticity (normalized by f); (d) horizontal structure of current phase and local wavenumbers; (e) kinetic energy transfer T_{KE} (positive from wave to mean flow); and (f) temporal evolution of amplitude (thin line) and instantaneous period (bold line). The dashed line in (f) and bold vector in (d) show the period and wavenumber obtained from the RT, respectively. The bold green line in (b) indicates an exponentially decaying profile, and the thin red line indicates a linearly decaying profile for a mean current that would permit surface boundary waves with characteristics similar to those observed.

below a surface layer ~40 m thick, decaying with an e-folding scale $H = 33$ m within the top 100 m. The amplitude reached a secondary maximum around 200 m. The mean currents were strongly sheared in the top 100 m as well.

The orientations of the waves' currents with respect to the horizontally sheared mean flow suggest that transfers of kinetic energy occurred between the waves and the mean flow (e.g., Kundu 1990, 429–436),

$$T_{KE} = \rho_0 \left[\overline{u'^2} \frac{\partial U}{\partial x} + \overline{u'v'} \left(\frac{\partial U}{\partial y} + \frac{\partial V}{\partial x} \right) + \overline{v'^2} \frac{\partial V}{\partial y} \right]; \quad (1)$$

T_{KE} was positive over most of the domain during period 1 (Fig. 3e), corresponding to a kinetic energy transfer from the wave to the mean flow. However, during period 2, T_{KE} was weaker and displayed areas of both signs (Fig. 4e).

4. Discussion

The most striking feature of these Rossby waves is their eastward zonal phase velocity. Indeed, the dispersion relation for free linear Rossby waves propagating in

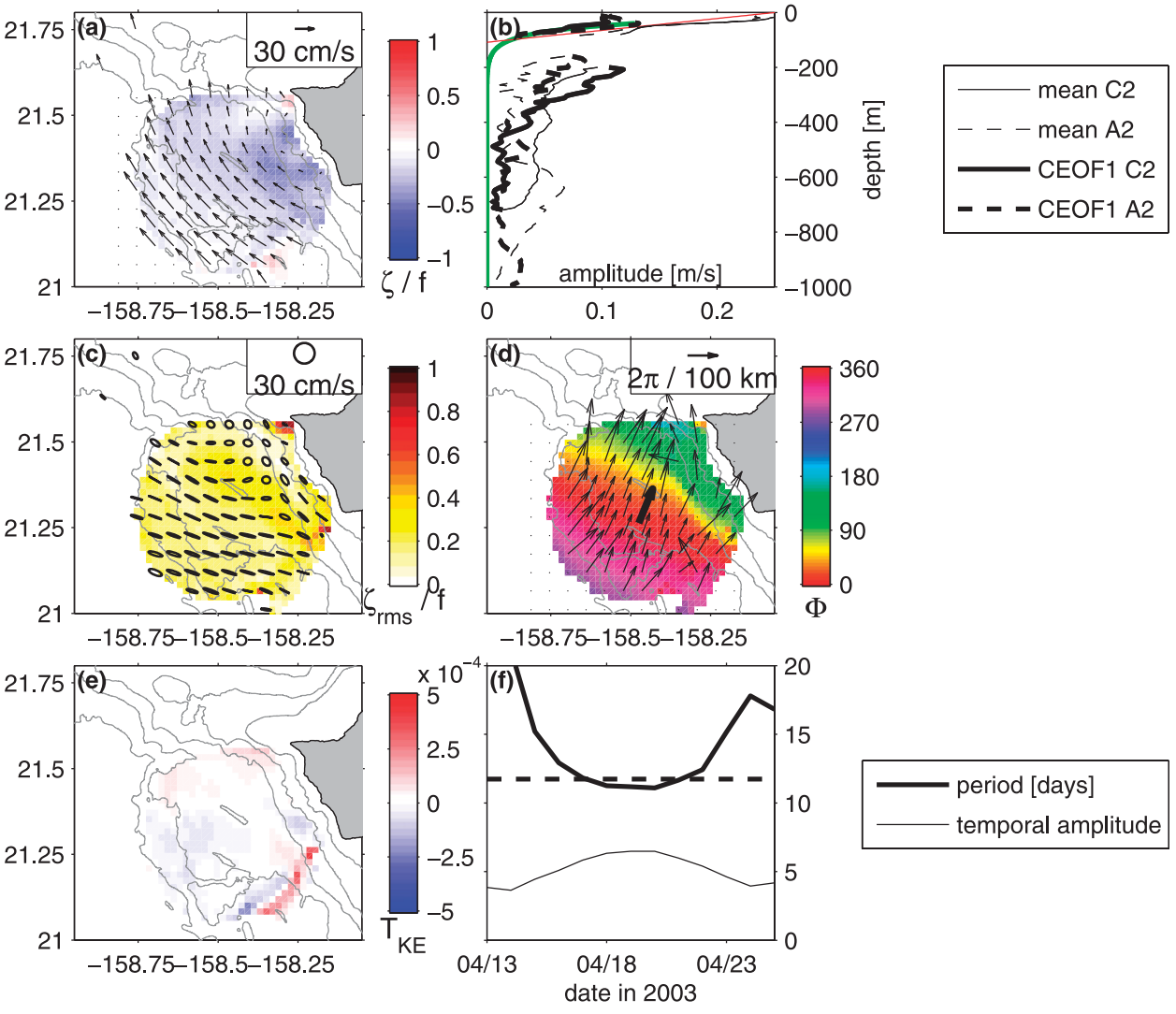

FIG. 4. As in Fig. 3, but for period 2.

a flat-bottomed β-plane ocean at rest is (e.g., Gill 1982, p. 500):

$$\omega = -k\frac{\beta}{k^2 + l^2 + \gamma^2}, \tag{2}$$

where ω is the frequency, k and l are the wavenumber zonal and meridional components, and $\gamma = (60\ \text{km})^{-1}$ is the inverse of the deformation radius (Chelton et al. 1998). The zonal phase velocity $c_p^x = \omega/k$ is westward ($c_p^x < 0$).

When the bottom is not flat, barotropic and bottom-trapped topographic Rossby waves can have an eastward zonal phase velocity if the bottom slopes down northward, opposing the β effect. However, surface-intensified baroclinic modes, such as those observed here (Figs. 3b, 4b), always have a westward zonal phase velocity (Rhines 1970; Straub 1994).

In the presence of a uniform zonal mean current U, the dispersion relation for free linear Rossby waves becomes (e.g., Vallis 2006, p. 231)

$$\omega = Uk - k\frac{\beta + U\gamma^2}{k^2 + l^2 + \gamma^2}. \tag{3}$$

The first term on the rhs of (3) is the Doppler shift, and $\hat{\beta} = \beta + U\gamma^2$ is the meridional gradient of background potential vorticity. The zonal phase velocity can be eastward in the presence of a sufficiently strong eastward mean current [$U > \beta/(k^2 + l^2)$], but the observed zonal background currents were westward during the passage of the waves (Figs. 3a, 4a).

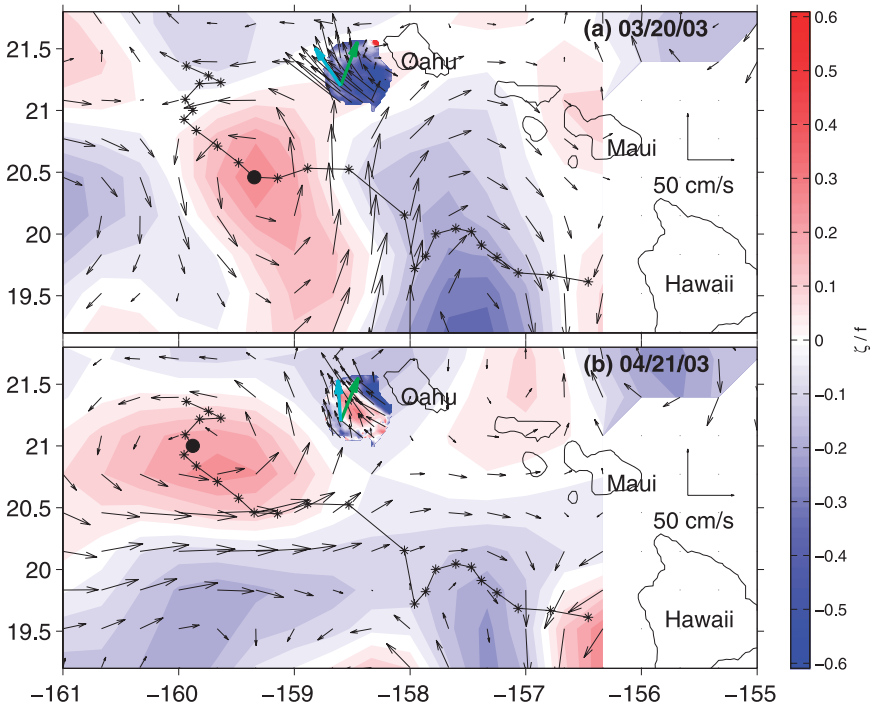

FIG. 5. Weekly averaged geostrophic currents from altimetry, centered on (a) 20 Mar and (b) 21 Apr 2003. The VRWs, absent from the gridded altimetric observations but resolved by the HFRs, are superimposed. Vorticity is normalized by f. The green arrows indicate the direction of phase propagation inferred from the RTs, and the cyan arrows indicate the group velocity inferred from the dispersion relation of VRWs. The track of the cyclone center is shown in black, with stars every 7 days, and the black bullets indicate the center's position at the times of the snapshots.

However, the background currents were not purely zonal and not uniform, being associated with the mesoscale cyclone observed by altimetry southwest of Oahu (Fig. 5). With a barotropic vortex on a shallow-water f plane, Montgomery and Kallenbach (1997) derived a dispersion relation for waves with horizontal scales smaller than the vortex radius, using a Wentzel–Kramers–Brillouin (WKB) approximation (i.e., assuming that the background state is constant over the scales of the waves). Here, we will use the quasigeostrophic version of McWilliams et al. (2003), because the Rossby number $\mathrm{Ro} = |\zeta/f|$ of the mesoscale cyclone is small (Fig. 5):

$$\omega = Vl + l\frac{\partial\zeta/\partial r - V\gamma^2}{k^2 + l^2 + \gamma^2}, \tag{4}$$

where k and l are the local wavenumber radial and azimuthal components, V is the vortex azimuthal velocity, and $\zeta = \partial(rV)/(r\partial r)$ is the relative vorticity. The expression $G = \partial\zeta/\partial r - V\gamma^2$ is the radial gradient of background potential vorticity, which replaces $\hat{\beta}$ in Eq. (3).

The terms V, ζ, and G were computed from the altimetric observations (Fig. 6) by defining the cyclone center as the velocity minimum and azimuthally averaging the azimuthal velocity. The HFR currents were also azimuthally averaged over the HFR domain. Differences between the altimetric and HFR radial profiles of azimuthal velocity may result from the 200-km objective mapping filter used to grid sea level anomalies (Ducet et al. 2000) and from the limited azimuthal range of the HFR domain. The value of ζ (Fig. 6b) was positive within 110 km from the center and negative farther away. The value of G (Fig. 6c) was negative everywhere and much stronger than β, justifying the f-plane approximation used to derive (4).

The velocity field of the cyclone varied significantly over $L = O(100)$ km, so that a strict WKB approximation does not hold. Nevertheless, a local frequency from (4) can be estimated at each grid point by using the local wavenumbers obtained from the CEOFs and the characteristics of the vortex at the corresponding ranges. The median of wave periods over all grid points from altimetry (HFR) are 20.2 (15.5) days for period 1 and 11.1 (8.6) days for period 2. Frequencies are dominated by the Doppler shift term and therefore are not too sensitive to the radial gradients of potential vorticity

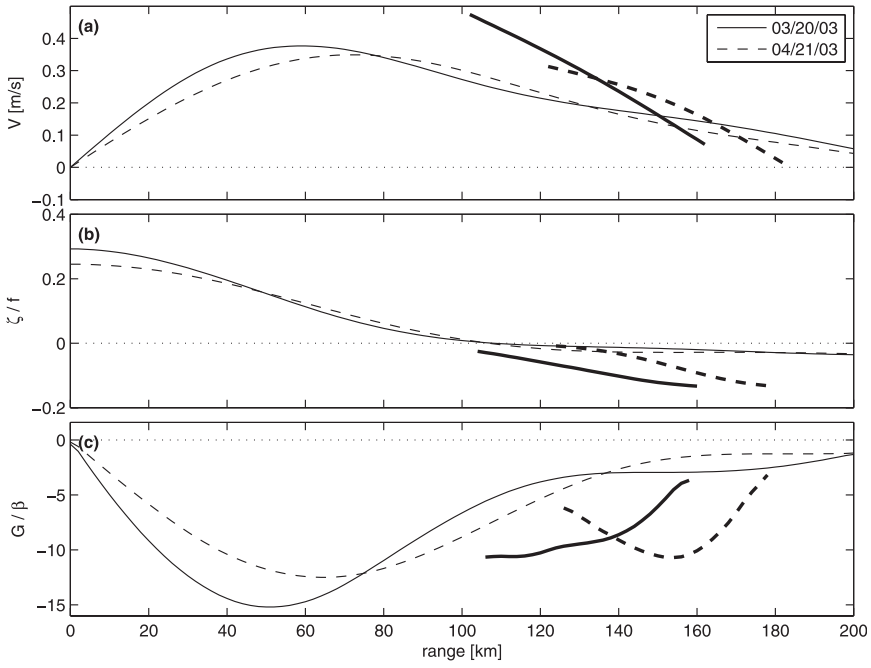

FIG. 6. Radial profiles, as a function of distance from the center of the cyclone, of azimuthally averaged (a) azimuthal velocity V (m s^{-1}); (b) relative vorticity ζ, normalized by f; and (c) radial gradient of potential vorticity G, normalized by β. Currents from altimetry (thin lines) and HFRs (bold lines) are shown for 20 Mar (solid lines) and 21 Apr (dashed lines). The HFR currents were averaged over the periods of the waves shown in Fig. 2.

which are necessary for the propagation of the waves. These values are close to those obtained from the RT and CEOF analyses. The waves therefore satisfy approximately the dispersion relation of VRWs. The observed decrease of wavelength with time (from 102 km during period 1 to 87 km during period 2) is also consistent with the continuous shearing of the waves by the differential azimuthal flow of the vortex (Montgomery and Kallenbach 1997; McWilliams et al. 2003). The transfer of kinetic energy from the wave to the mean flow observed in March is also consistent with vortex strengthening resulting from wave-mean flow interactions seen in numerical simulations (Montgomery and Kallenbach 1997; Möller and Montgomery 1999; McWilliams et al. 2003; Graves et al. 2006).

Group velocities can be obtained from (4), and their median values over all grid points are shown in Fig. 5 (cyan arrows). Although the phase was propagating into the coast of Oahu, the energy was propagating almost parallel to the coast, precluding reflections that would have otherwise distorted the phase patterns.

Equation (4) was derived for an equivalent barotropic vortex. This is a reasonable approximation during period 1 (Fig. 3b), but the mean vertical shear cannot be ignored during period 2 (Fig. 4b). Its effects are illustrated by the idealized case of a horizontally homogeneous mean flow with constant vertical shear U_z, $U(z) = U_0 + U_z z$, where U_0 is the surface current. For constant buoyancy frequency N, the quasigeostrophic problem has a surface-trapped solution with a dispersion relation of the form (Pedlosky 2003, 211–212)

$$\omega = kU_0 - \frac{kfU_z}{KN}, \tag{5}$$

where (k, l) is the wavenumber expressed in a Cartesian coordinate system aligned with the mean flow and $K = (k^2 + l^2)^{1/2}$. The wave amplitude decays exponentially with depth, with an e-folding scale $H = f/(KN)$. The term U_0 was obtained by spatially averaging the mean HFR currents, k and ω were taken from the RTs, and H was obtained from the CEOF vertical profiles to yield U_z from (5). The resulting profiles are shown in Figs. 3b and 4b (thin red lines). Although the required shear is stronger than the observed shear during period 1, the agreement in the top 100 m is better during period 2. Therefore, during period 2, the wave also satisfies the dispersion relation of surface boundary waves permitted by the mean vertical shear.

These observations provide evidence for the existence of VRWs, the dynamics of which depends on advection and vorticity gradients created by mesoscale eddies. The

HFRs provided high-horizontal-resolution data, complementing the ADCPs' vertical resolution, to support the VRW hypothesis that would otherwise have been difficult to test. VRWs may be ubiquitous in the ocean and may simply have gone undetected because of the lack of appropriate observations.

Acknowledgments. We thank Paolo Cipollini, Eric Firing, Mark Merrifield, and Michael Montgomery for fruitful scientific discussions and two anonymous reviewers, who helped to clarify the manuscript. The moorings, the HFRs, and their deployment were funded by the National Science Foundation; full acknowledgments can be found in Chavanne et al. (2010b). P. Flament and D. Luther are also supported by the State of Hawaii. This publication was prepared under Cooperative Agreement NA07NOS4730207 from the National Oceanographic and Atmospheric Administration Integrated Ocean Observing System Program Office, U.S. Department of Commerce.

REFERENCES

Barnett, T. P., 1983: Interaction of the monsoon and Pacific trade wind system at interannual time scales. Part I: The equatorial zone. *Mon. Wea. Rev.,* **111,** 756–773.

Challenor, P. G., P. Cipollini, and D. Cromwell, 2001: Use of the 3D Radon transform to examine the properties of oceanic Rossby waves. *J. Atmos. Oceanic Technol.,* **18,** 1558–1566.

Chavanne, C., P. Flament, and K.-W. Gurgel, 2010a: Interactions between a submesoscale anticyclonic vortex and a front. *J. Phys. Oceanogr.,* **40,** 1802–1818.

——, ——, E. Zaron, G. Carter, M. Merrifield, D. Luther, and K.-W. Gurgel, 2010b: The surface expression of semidiurnal internal tides near a strong source at Hawaii. Part I: Observations and numerical predictions. *J. Phys. Oceanogr.,* **40,** 1155–1179.

Chave, A. D., D. S. Luther, and J. H. Filloux, 1992: The Barotropic Electromagnetic and Pressure Experiment 1. Barotropic current response to atmospheric forcing. *J. Geophys. Res.,* **97** (C6), 9565–9593.

Chelton, D. B., and M. G. Schlax, 1996: Global observations of oceanic Rossby waves. *Science,* **272,** 234–238.

——, R. A. deSzoeke, M. G. Schlax, K. El Naggar, and N. Siwertz, 1998: Geographical variability of the first baroclinic Rossby radius of deformation. *J. Phys. Oceanogr.,* **28,** 433–460.

Ducet, N., P. Y. L. Traon, and G. Reverdin, 2000: Global high-resolution mapping of ocean circulation from TOPEX/Poseidon and ERS-1 and -2. *J. Geophys. Res.,* **105** (C8), 19 477–19 498.

Gill, A. E., 1982: *Atmosphere–Ocean Dynamics*. Academic Press, 662 pp.

Graves, L. P., J. C. McWilliams, and M. T. Montgomery, 2006: Vortex evolution due to straining: A mechanism for dominance of strong, interior anticyclones. *Geophys. Astrophys. Fluid Dyn.,* **100,** 151–183.

Hansen, D. V., 1970: Gulf Stream meanders between Cape Hatteras and the Grand Banks. *Deep-Sea Res.,* **17,** 495–511.

Kundu, P. K., 1990: *Fluid Mechanics*. Academic Press, 638 pp.

MacDonald, N. J., 1968: The evidence for the existence of Rossby-like waves in the hurricane vortex. *Tellus,* **20,** 138–150.

McWilliams, J. C., L. P. Graves, and M. T. Montgomery, 2003: A formal theory for vortex Rossby waves and vortex evolution. *Geophys. Astrophys. Fluid Dyn.,* **97,** 275–309.

Möller, J. D., and M. T. Montgomery, 1999: Vortex Rossby waves and hurricane intensification in a barotropic model. *J. Atmos. Sci.,* **56,** 1674–1687.

Montgomery, M. T., and R. J. Kallenbach, 1997: A theory for vortex Rossby-waves and its application to spiral bands and intensity changes in hurricanes. *Quart. J. Roy. Meteor. Soc.,* **123,** 435–465.

Pedlosky, J., 2003: *Waves in the Ocean and Atmosphere: Introduction to Wave Dynamics*. Springer, 260 pp.

Reasor, P. D., and M. T. Montgomery, 2001: Three-dimensional alignment and corotation of weak, TC-like vortices via linear vortex Rossby waves. *J. Atmos. Sci.,* **58,** 2306–2330.

Rhines, P., 1970: Edge-, bottom-, and Rossby waves in a rotating stratified fluid. *Geophys. Fluid Dyn.,* **1,** 273–302.

Straub, D. N., 1994: Dispersive effects of zonally varying topography on quasigeostrophic Rossby waves. *Geophys. Astrophys. Fluid Dyn.,* **75,** 107–130.

Tracey, K. L., D. R. Watts, C. S. Meinen, and D. S. Luther, 2006: Synoptic maps of temperature and velocity within the Subantarctic Front south of Australia. *J. Geophys. Res.,* **111,** C10016, doi:10.1029/2005JC002905.

Vallis, G. K., 2006: *Atmospheric and Oceanic Fluid Dynamics: Fundamentals and Large-Scale Circulation*. Cambridge University Press, 745 pp.

White, W. B., 1977: Annual forcing of baroclinic long waves in the tropical North Pacific Ocean. *J. Phys. Oceanogr.,* **7,** 50–61.